



HAL
open science

Experimental Characterization of a Circularly-Polarized 1-Bit Unit-Cell for Beam Steerable Transmitarrays at Ka-Band

Luca Di Palma, Antonio Clemente, Laurent Dussopt, Ronan Sauleau, Patrick
Potier, Philippe Pouliguen

► **To cite this version:**

Luca Di Palma, Antonio Clemente, Laurent Dussopt, Ronan Sauleau, Patrick Potier, et al.. Experimental Characterization of a Circularly-Polarized 1-Bit Unit-Cell for Beam Steerable Transmitarrays at Ka-Band. *IEEE Transactions on Antennas and Propagation*, 2019, 67 (2), pp.1300-1305. 10.1109/TAP.2018.2880095 . hal-01987895

HAL Id: hal-01987895

<https://univ-rennes.hal.science/hal-01987895>

Submitted on 24 Jan 2019

HAL is a multi-disciplinary open access archive for the deposit and dissemination of scientific research documents, whether they are published or not. The documents may come from teaching and research institutions in France or abroad, or from public or private research centers.

L'archive ouverte pluridisciplinaire **HAL**, est destinée au dépôt et à la diffusion de documents scientifiques de niveau recherche, publiés ou non, émanant des établissements d'enseignement et de recherche français ou étrangers, des laboratoires publics ou privés.

Experimental Characterization of a Circularly-Polarized 1-Bit Unit-Cell for Beam Steerable Transmitarrays at Ka-Band

Luca Di Palma, *Member, IEEE*, Antonio Clemente, *Senior Member, IEEE*, Laurent Dussopt, *Senior Member, IEEE*, Ronan Sauleau, *Fellow, IEEE*, Patrick Potier, and Philippe Pouliguen

Abstract— We propose here an experimental characterization procedure applied to a 1-bit reconfigurable transmitarray unit-cell working in circular polarization at Ka-band. The transmission phase of the unit-cell is controlled on the receiving side by switching two p-i-n diodes integrated on the radiating element. The circular polarization is generated on the transmitting side with a truncated corner patch antenna. A specific waveguide characterization setup and related procedure have been developed to extract the unit-cell S-matrix. The proposed setup includes non-standard waveguide sections, ad-hoc transitions and an Ortho-Mode Transducer (OMT). The experimental results demonstrate a good agreement with full-wave simulations with a discrepancy of less than 0.1 dB on the measured minimum insertion loss of 1.65 dB at 29 GHz. A 3-dB bandwidth larger than 12% has been measured.

Index Terms— Waveguide simulator, circular polarization, transmitarray antenna, discrete lens, array lens, Ka-band.

I. INTRODUCTION

TRANSMITARRAYS have been massively studied in the last years for applications up to the sub-millimeter-wave band [1]-[2]. Even if several high-performance fixed-beam transmitarrays have been successfully demonstrated, only a few demonstrations of full electronically reconfigurable transmitarrays have been presented in the open literature [3]-[5]. In our recent paper [3], we implemented a circularly-polarized (CP) electronically reconfigurable transmitarray based on a sequentially-rotated linearly-polarized (LP) 1-bit unit-cell [6] enabling simple polarization switching. This transmitarray exhibits a significant directivity loss due to the generation of the circular polarization from the sequential rotation of orthogonal LP unit cells. Circularly-polarized unit-cells are therefore proposed in the literature in order to improve the aperture efficiency. However, to our knowledge, there is no experimental characterization technique in waveguide environment published so far for CP unit-cells, in contrast to LP unit-cells [7], which can be characterized with standard rectangular waveguides and 2-port TRL calibration. In [8], a CP unit-cell has been characterized in free-space at

X-band. In this paper, we describe an experimental characterization procedure based on waveguide simulators for transmitarray unit-cells working in circular polarization. The proposed method allows to verify the transmitarray performance at unit-cell level during preliminary development phases. This enables to individuate possible issue and re-optimize the design without the need of manufacturing and anechoic chamber test of the whole transmitarray panel that often consists of thousands of elements. This possibility is even more useful for reconfigurable CP unit-cell designs whose layout is more complex and requires integration of one or more active components.

This paper is organized as follows. In Section II, the unit-cell architecture detailed in our previous paper [9] is briefly recalled. The proposed characterization setup and measurement procedures are described in detail in Section III, and experimental results are provided in Section IV. Finally, conclusions are drawn in Section V.

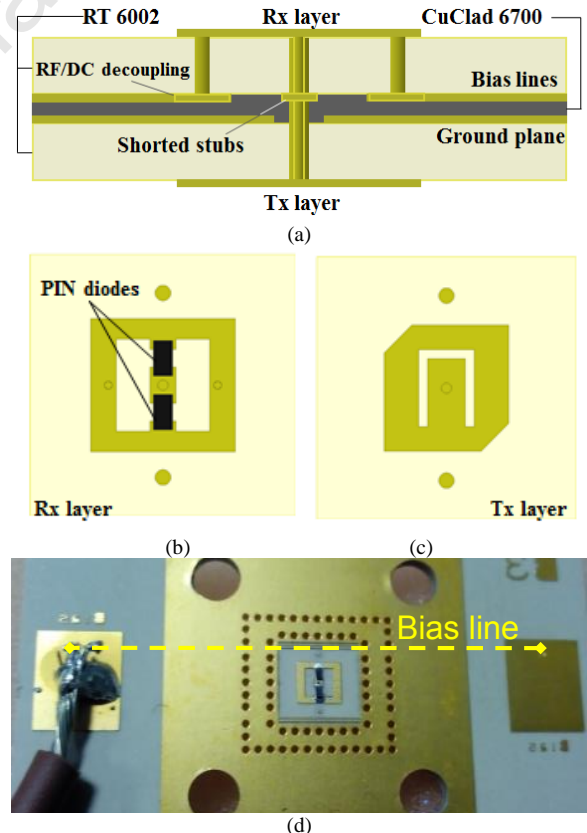


Fig. 1. Designed and fabricated 1-bit CP unit-cell operating at Ka-band: (a) PCB stack-up; sketch of the (b) receiving (Rx) and (c) transmitting (Tx) layers. These figures are similar to the ones published in [9], where further details on the architecture are given, but are reported here to facilitate the reader understanding. (d) Photograph of the realized prototype (Rx layer).

Manuscript received on May 7, 2018. This work has been partly funded by the Direction Générale de l'Armement (DGA/DS/MRIS), France.

L. Di Palma, A. Clemente and L. Dussopt are with CEA-LETI, Minatec Campus, F38054 Grenoble, France (e-mail: antonio.clemente@cea.fr, laurent.dussopt@cea.fr).

R. Sauleau is with the Institut d'Electronique et de Télécommunications de Rennes (IETR), UMR CNRS 6164, Université de Rennes 1, F35042, Rennes, France (e-mail: ronan.sauleau@univ-rennes1.fr).

P. Potier is with the Direction Générale de l'Armement (DGA), F-35174, Bruz cedex, France (e-mail: patrick.potier@intra.def.gouv.fr).

P. Pouliguen is with the Direction Générale de l'Armement (DGA), Strategy Directorate, Office for Advanced Research and Innovation, F-92221 Bagneux cedex, France (e-mail: philippe.pouliguen@intra.def.gouv.fr).

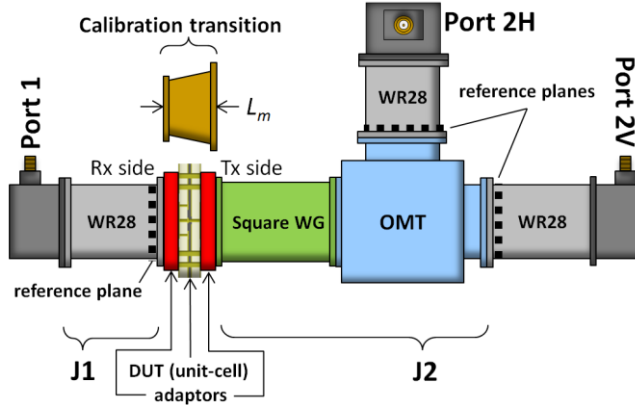


Fig. 2. Scheme of the waveguide simulator set-up proposed to characterize the CP unit-cell. It is formed by a WR28 straight section (junction J1), DUT (unit-cell) with *ad-hoc* adaptors (in red), a square waveguide straight section and an OMT junction to separate linear horizontal (H) and vertical (V) polarizations. Reference planes related to TRL procedure performed in calibration step 1 are shown with dashed bold lines. During calibration procedure the DUT is replaced by a calibration transition of length $L_m = 9$ mm (calibration steps 2-4).

II. ARCHITECTURE OF THE 1-BIT UNIT-CELL

The unit-cell operates at Ka-band (27.5 GHz - 31.0 GHz), and its size is 5.1×5.1 mm² ($\lambda_0/2 \times \lambda_0/2$, where λ_0 is the wavelength in free space at 29.4 GHz). It has been designed on the dielectric stack-up shown in Fig. 1a and formed by two identical substrates (Rogers Duroid RT6002, thickness 508 μ m, $\epsilon_r = 2.94$), a bonding film (Arlon CuClad 6700, thickness 114 μ m, $\epsilon_r = 2.30$) and four metal layers. The receiving (Rx) layer is composed of a rectangular patch loaded by an O-shaped slot and two p-i-n diodes (Fig. 1b); this active patch is linearly-polarized. It is worth to notice that this choice allows the use of a simple and wideband LP focal source. In the transmitting layer (Tx), a square patch loaded by a U-shaped slot with truncated corners is designed in order to generate circular polarization (Fig. 1c).

The active patch is connected to the passive one with a metallized via hole placed at the center of the unit-cell. A ground plane occupies one of the two intermediate metallic layers. The other inner layer, shown in Fig. 1a, is used to route the DC bias network. The ground connection is realized with two symmetrical short-circuited quarter-wavelength stubs connected to the central via hole.

This unit-cell has been simulated and optimized using the commercial software Ansys HFSS with periodic boundary conditions and Floquet port excitations. More details on the simulation results and p-i-n diode models are available in our previous works [6], [7], [9]. A photograph of the realized prototype is reported in Fig. 1d.

III. EXPERIMENTAL CHARACTERIZATION OF THE CIRCULARLY-POLARIZED UNIT-CELL

A. Characterization setup

The proposed measurement waveguide simulator set-up is outlined in Fig. 2. It is formed by two junctions: J1 (from the

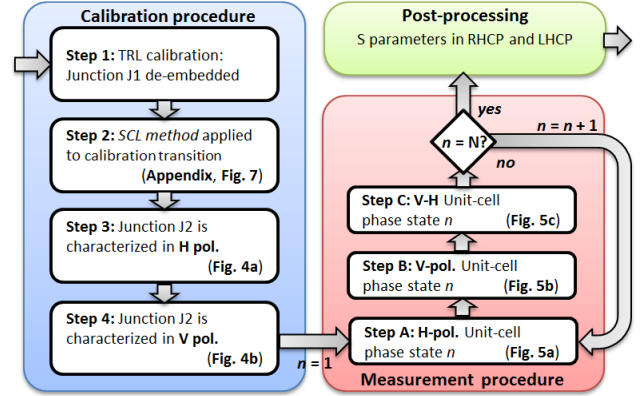


Fig. 3. Block diagram of the proposed characterization method. It includes calibration, measurement and post-processing phases. All the steps contained in the measurement procedure are repeated N times, where N is the number of phase states of the DUT. For the tested case: $N = 2$ (phase states: $0^\circ/180^\circ$).

Rx side) and J2 (from the Tx side). The unit-cell is connected between the two junctions through short *ad-hoc* tapered adaptors (represented in red in Fig. 2) of length equal to 1.2 mm ($\lambda_0/8.6$) to match the waveguide dimensions to the unit-cell size. They cannot be de-embedded since the sizes of the transverse sections (5.1×5.1 mm²) connected to the unit-cell do not allow propagation of the fundamental mode. However, similar adaptors have been already proposed for LP unit-cell characterization in [6]. Their role is mainly to minimize the impedance mismatch between the unit-cell section and the waveguides.

The junction J1 is formed by a standard WR28 rectangular waveguide section (7.112×3.556 mm²). The junction J2 includes a square non-standard waveguide connected to the Tx side of the unit-cell enabling the propagation of two orthogonal fundamental modes. A side of 6.5 mm has been selected in order to have a single mode ($f_c^{\text{TE}_{10}/\text{TE}_{01}} = 23.1$ GHz) within the working band and avoid higher-order modes ($f_c^{\text{TE}_{11}/\text{TM}_{11}} = 32.6$ GHz). This square waveguide is connected to an orthomode transducer (OMT) in order to separate the two orthogonal vertical (V) and horizontal (H) components. A commercial OMT manufactured by MM Microwave [10] with nominal working band between 27.0 and 31.0 GHz (return loss R.L. > 10 dB, insertion loss I.L. < 1.5 dB, isolation > 30 dB) has been selected. Its scattering matrix can be defined as follows:

$$\underline{\underline{S}}^{J2} = \begin{pmatrix} S_{1H1H}^{J2} & S_{1H2H}^{J2} & 0 & 0 \\ S_{2H1H}^{J2} & S_{2H2H}^{J2} & 0 & 0 \\ 0 & 0 & S_{1V1V}^{J2} & S_{1V2V}^{J2} \\ 0 & 0 & S_{2V1V}^{J2} & S_{2V2V}^{J2} \end{pmatrix} = \begin{pmatrix} \underline{\underline{S}}_H^{J2} & 0_{2,2} \\ 0_{2,2} & \underline{\underline{S}}_V^{J2} \end{pmatrix}, \quad (1)$$

where numbers 1, 2 denote the set-up ports defined in Fig. 2, and letters H and V refer, respectively, to the two horizontal and vertical orthogonal polarizations only defined at port 2.

By inserting the null elements in the matrix of Eq. (1), we assumed ideal isolation between the orthogonal modes separated by the OMT. With the actual OMT, this is not strictly true and leads to a systematic error that cannot be de-

embedded. However, if the OMT exhibits a high isolation (greater than 30 dB, as this is the case here) in the frequency band of interest, the impact of this approximation on the measurement accuracy is very limited. Therefore, junction J2 can be represented by two independent 2-port scattering matrices \underline{S}_H^{J2} and \underline{S}_V^{J2} , one for each polarization, that are measured in the calibration procedure described in the following section. These two matrices can be also represented by transfer (ABCD) matrices \underline{T}_H^{J2} and \underline{T}_V^{J2} respectively.

B. Calibration procedure

Several steps are needed for the calibration of the proposed setup of Fig. 2; they are summarized in Fig. 3. Each one is detailed in the following.

1) Calibration Step 1

A two-port TRL (Thru-Reflect-Line) calibration procedure is performed to de-embed the coaxial adaptors and the standard WR28 rectangular straight sections. A short circuit and a 3.56-mm-thick shim are used as reflect and line standard, respectively. The reference planes resulting from this operation are highlighted with dashed bold lines in Fig. 2. In this way, junction J1 is fully de-embedded.

2) Calibration Step 2

An *ad-hoc* calibration transition (see Fig. 2) from WR-28 to a square waveguide has been designed in order to interface a standard waveguide with the square port of junction J2 and allow its characterization (in Calibration Step 3). This calibration transition is characterized using the Short Circuit Line (SCL) method, which is reported in detail in the Appendix [11]-[13]. As a result, the scattering (transfer) matrix $\underline{S}^{cal}(\underline{T}^{cal})$ of this calibration transition is obtained.

3) Calibration Step 3

The characterized calibration transition is connected to the junction J2, as shown in Fig. 4a. The transmission matrix

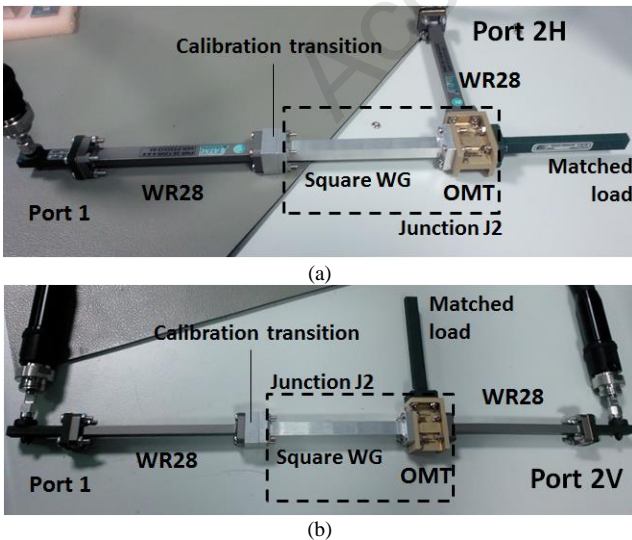


Fig. 4: Photographs of the waveguide setup for calibration steps (a) 3 and (b) 4, described in Section III-B. Junction J2 is connected to a calibration transition of length $L_m = 9$ mm, that was previously characterized with the SCL method (see Appendix).

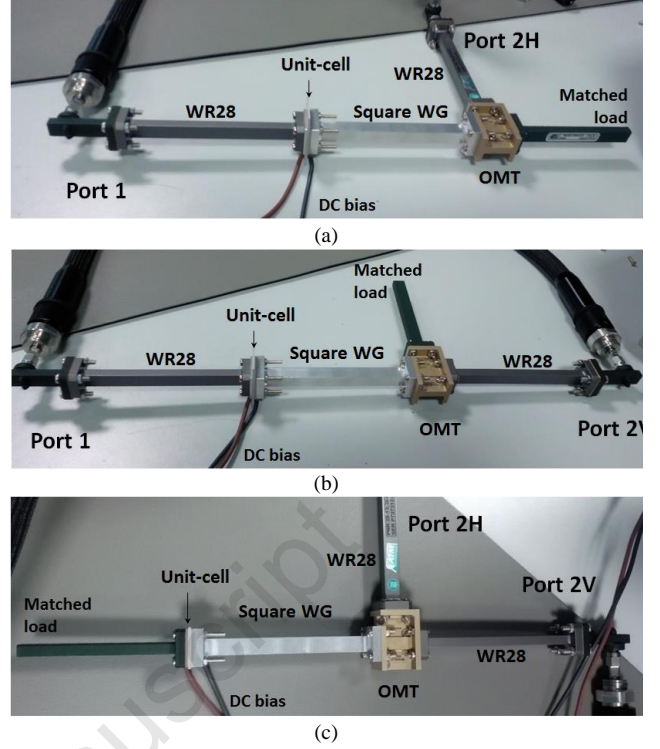


Fig. 5: Photographs of the waveguide setup for measurement steps (a) A, (b) B and (c) C, described in Section III-C.

$\underline{T}_{meas,H}^{J2}$ associated to the horizontal polarization is measured between port 1 and port 2H. Since we used a two-port vector network analyzer, the third port (2V) of J2 was loaded by a matched load. By de-embedding the transition from the measurement data, we obtain

$$\underline{T}_H^{J2} = \underline{T}_{meas,H}^{J2} \cdot (\underline{T}^{cal})^{-1}. \quad (2)$$

4) Calibration Step 4

The scattering parameters associated to the vertical polarization are measured by rotating by 90° the calibration transition and connecting it to junction J2. Port 2H is now connected to a matched load, as shown in Fig. 4b. De-embedding the calibration transition from the measurement data allows to derive

$$\underline{T}_V^{J2} = \underline{T}_{meas,V}^{J2} \cdot (\underline{T}^{cal})^{-1}. \quad (3)$$

To conclude, with the measurements performed in the calibration steps 2-4, the scattering matrix of junction J2 reported in Eq. (1) is fully known.

C. Measurement procedure

Once the calibration steps are completed, the following S parameters must be extracted in order to fully characterize the DUT

$$\underline{S}^{cell} = \begin{pmatrix} S_{2H2H}^{cell} & S_{2H2V}^{cell} & S_{2V2H}^{cell} \\ S_{12H}^{cell} & S_{11}^{cell} & S_{12V}^{cell} \\ S_{2V2H}^{cell} & S_{2V2V}^{cell} & S_{2V2V}^{cell} \end{pmatrix}. \quad (4)$$

The adopted notation is coherent with the one defined previously in Eq. (1). Port 1 in this case is defined only for vertical polarization (V) and the associated subscript is omitted.

For a DUT having N phase states, all the measurement steps described in the following must be repeated N times. For the two-state ($0^\circ/180^\circ$) unit-cell described in Section II, the measurement procedure is performed twice ($N = 2$).

The S parameters contained in Eq. (4) can be re-arranged in three 2-port S-matrices

$$\underline{\underline{S}}_V^{cell} = \begin{pmatrix} S_{11}^{cell} & S_{12V}^{cell} \\ S_{2V1}^{cell} & S_{2V2V}^{cell} \end{pmatrix}, \underline{\underline{S}}_H^{cell} = \begin{pmatrix} S_{11}^{cell} & S_{12H}^{cell} \\ S_{2H1}^{cell} & S_{2H2H}^{cell} \end{pmatrix}, \quad (5)$$

$$\underline{\underline{S}}_{VH}^{cell} = \begin{pmatrix} S_{2V2V}^{cell} & S_{2V2H}^{cell} \\ S_{2H2V}^{cell} & S_{2H2H}^{cell} \end{pmatrix}.$$

A transfer matrix ($\underline{\underline{T}}_V^{cell}, \underline{\underline{T}}_H^{cell}, \underline{\underline{T}}_{VH}^{cell}$) can be associated to each of these matrices by applying the well-known conversion rules. Therefore, three 2-port measurements (Fig. 5) are performed on the setup in order to extract these three matrices, as detailed in the following steps.

1) Measurement A

The first measurement is performed to extract parameters included in $\underline{\underline{S}}_H^{cell}$ and associated to the horizontal polarization (Eq. (5)). The matched load is connected to Port 2V (Fig. 5a). Using the transfer matrix notation, we have

$$\underline{\underline{T}}_H^{cell} = \underline{\underline{T}}_{meas,H} \cdot (\underline{\underline{T}}_H^{J2})^{-1}, \quad (6)$$

where $\underline{\underline{T}}_{meas,H}$ is the measured transfer matrix associated to the setup reported in Fig. 5a.

2) Measurement B

A second measurement is done to retrieve parameters of $\underline{\underline{S}}_V^{cell}$ related to the vertical polarization (Eq. (5)). The matched load has been connected this time to Port 2H (Fig. 5b). Using the transfer matrix notation, we have

$$\underline{\underline{T}}_V^{cell} = \underline{\underline{T}}_{meas,V} \cdot (\underline{\underline{T}}_V^{J2})^{-1}, \quad (7)$$

where $\underline{\underline{T}}_{meas,V}$ is the measured transmission matrix.

3) Measurement C

Finally, a third measurement is performed to evaluate the S matrix $\underline{\underline{S}}_{VH}^{cell}$ associated to the horizontal-vertical polarization at port 2 (Eq. (5)). The matched load is connected this time to Port 1V (Fig. 5c). Using the transfer matrix notation, we have

$$\underline{\underline{T}}_{VH}^{cell} = (\underline{\underline{T}}_V^{J2})^{-1} \cdot \underline{\underline{T}}_{meas,VH} \cdot (\underline{\underline{T}}_H^{J2})^{-1}, \quad (8)$$

where $\underline{\underline{T}}_{meas,HV}$ is the measured transmission matrix.

D. Post-processing

Finally, S-parameters contained in Eq. (4) can be calculated starting from the 2-port transfer matrices of Eq. (6)-(8). The obtained parameters (magnitude and phase) for vertical and horizontal polarizations must be properly combined with a phase shift of $\pm 90^\circ$ for the CP components calculation. Denoting with L and R the $LHCP$ and $RHCP$ components, respectively, the following equations can be derived for the transmission coefficients

$$S_{2L1}^{cell} = \frac{1}{\sqrt{2}} (S_{2V1}^{cell} + jS_{2H1}^{cell}), \quad (9)$$

$$S_{2R1}^{cell} = \frac{1}{\sqrt{2}} (S_{2V1}^{cell} - jS_{2H1}^{cell}). \quad (10)$$

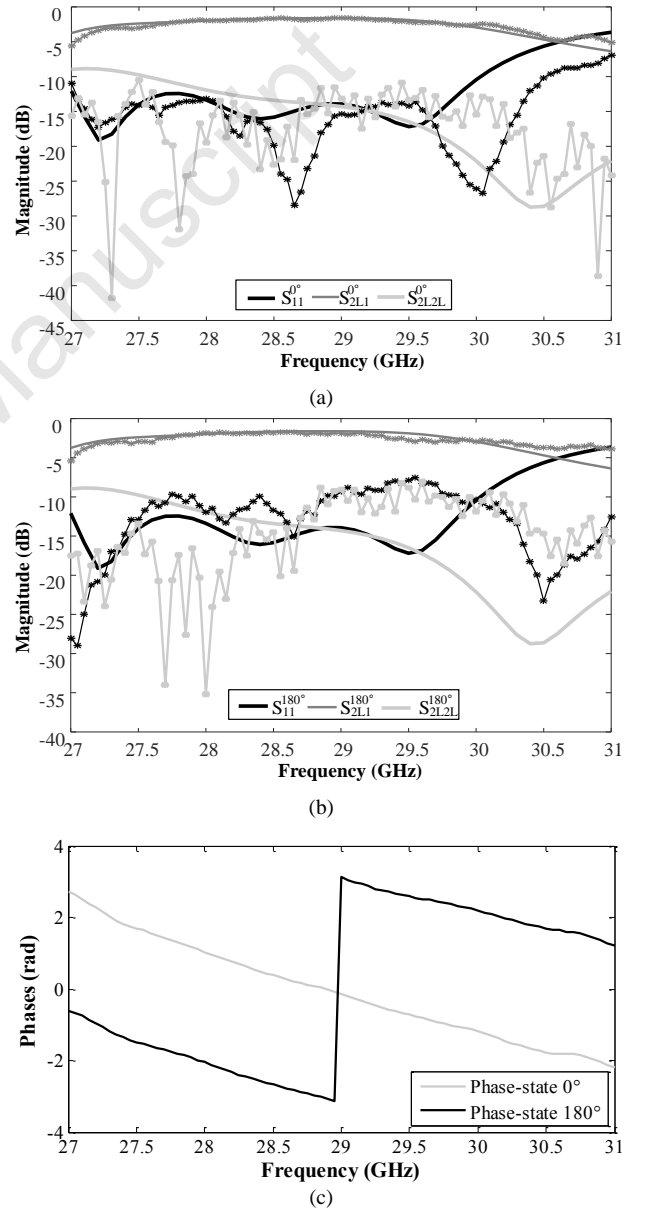


Fig. 6. Magnitude of the simulated (line) and measured (line and symbols) scattering parameters of the reconfigurable unit-cell. (a) Phase-state 0° and (b) phase state 180° . (c) Phase of the measured transmission coefficients of the reconfigurable unit-cell in both phase states.

TABLE I: SUMMARY OF THE CIRCULARLY-POLARIZED UNIT-CELL PERFORMANCES

	Phase-state 0°		Phase-state 180°	
	Simul.	Meas.	Simul.	Meas.
Min I.L. (dB)	1.61	1.59	1.61	1.70
1-dB BW (GHz/%)*	27.3-29.9	27.6-30.2	27.3-29.9	27.6-29.5
3-dB BW (GHz/%)*	26.9-30.5	27.0-30.5	26.9-30.5	27.0-31
	12.4	12.0	12.4	13.8

* Relative bandwidth has been calculated at 29 GHz.

While the reflection coefficient at port 1 is in LP, CP reflection coefficients can be defined at port 2 as follows

$$S_{2R2R}^{cell} = \frac{1}{2}(S_{2V2V}^{cell} + jS_{2V2H}^{cell} + jS_{2H2V}^{cell} - S_{2H2H}^{cell}), \quad (11)$$

$$S_{2R2L}^{cell} = \frac{1}{2}(S_{2V2V}^{cell} - jS_{2V2H}^{cell} - jS_{2H2V}^{cell} - S_{2H2H}^{cell}), \quad (12)$$

$$S_{2L2R}^{cell} = \frac{1}{2}(S_{2V2V}^{cell} + jS_{2V2H}^{cell} - jS_{2H2V}^{cell} + S_{2H2H}^{cell}), \quad (13)$$

$$S_{2L2L}^{cell} = \frac{1}{2}(S_{2V2V}^{cell} - jS_{2V2H}^{cell} + jS_{2H2V}^{cell} + S_{2H2H}^{cell}). \quad (14)$$

IV. MEASUREMENT RESULTS

In order to validate its design, the 1-bit unit-cell presented in Section II has been fully characterized with the methodology presented in Section III. The measurements have been compared with full-wave simulations of the unit-cell in a simplified version of the waveguide set-up reported in Fig. 2. In particular, junction J2 is reduced to only the square non-standard waveguide section and all the coaxial adapters are eliminated. With proper reference planes, this full-wave model corresponds ideally to the one obtained at the end of the proposed characterization procedure.

S-parameters are reported in Figs. 6(a) and 6(b) for the 0° and 180° phase states, respectively. In the case of the 0° phase state, a good agreement is observed between the transmission coefficients in the frequency band 27.2-30.65 GHz. The measured minimum I.L. is equal to 1.59 dB at 28.9 GHz with an error of less than 0.05 dB as compared to the simulated results. In the case of the 180° phase state, the measured minimum I.L. is equal to 1.70 dB at 28.5 GHz with a relative error lower than 0.1 dB. At the edge of the working band, the error on transmission coefficients is lower than 0.5 dB and 1.0 dB maximum for the 0° and 180° phase states, respectively. Larger discrepancies on the reflection coefficients can be observed. These errors are attributed mainly to the approximation done in the procedure (perfect isolation between the two LP OMT ports), and the random errors occurring during the multiple connections steps (e.g. alignment errors). In particular, a simpler procedure and a better accuracy would be expected using a three-port vector-network analyzer instead of a two-port one.

Finally, the phase of the unit-cell measured transmission coefficients is plotted in Fig. 6c. The plot shows that a relative phase shift of 180° with a maximum error of 13° and 17° is achieved on the frequency bands 27-30 GHz and 27-31 GHz, respectively. The unit-cell performance is summarized in

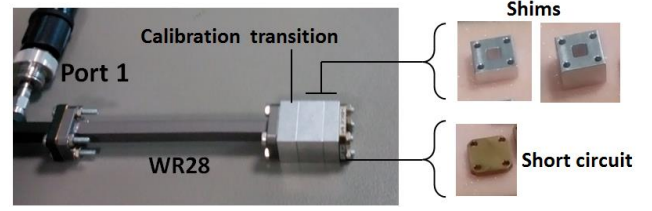


Fig. 7. Photograph of the experimental setup used for the characterization of the calibration transition with SCL method (calibration step 2). Two square waveguide shims of length $L_1 = 7$ mm and $L_2 = 12$ mm have been realized and connected to a short circuit. The third shim has been realized by cascading the two ($L_3 = L_1 + L_2$).

Table I.

V. CONCLUSION

In this paper, a method for the experimental characterization of transmitarray CP unit-cells with arbitrary phase resolution (N phase states) in a waveguide simulator with non-standard access ports has been proposed and successfully tested on a 1-bit ($N = 2$) tunable unit-cell designed in Ka-band. This method allows to assess CP unit-cell performance avoiding the prototyping of the whole antenna panel and to test further key parameters of reconfigurable architectures (e.g. power consumption, 1-dB compression point, dissipation, life cycle of active devices, etc.).

The main limitations are only represented by waveguide and OMT bandwidths. However, it is sufficient to carefully select these components on the basis of operative frequency range of the DUT. Unit-cells with ultra-wideband features can be eventually characterized in sub-bands by using ad-hoc multiple measurement setups with proper waveguide sizes and OMT junctions.

The calibration and measurement procedures, which include multiple junction de-embedding steps, have been described. A minimum insertion loss of about 1.65 dB at 29 GHz with a 3-dB relative bandwidth greater than 12% has been demonstrated in good agreement with simulation results. The obtained results validate both the proposed experimental characterization approach and the unit-cell design at Ka-band frequencies.

APPENDIX

The square-to-rectangular (WR-28) transition of length $L_m = 9$ mm employed in the calibration procedure steps 2-4 has been characterized with the Short Circuit Line (SCL) method. This method has been already used in the past for the characterization of material permittivity and permeability [11]-[13]. It consists in connecting a short circuit to one port of the device at several distances (three distances in our case: L_1, L_2, L_3), as illustrated in Fig. 7. Here, these three loads are implemented with a short circuit combined with two square-waveguide (6.5×6.5 mm²) shims. The reflection coefficients of these loads ($\Gamma_{L1}, \Gamma_{L2}, \Gamma_{L3}$) are supposed to be known with sufficient accuracy since in general they can be directly measured. In our case, the measurement of these loads would be complex because of the non-standard square waveguide. Instead, we considered an accurate full-wave model (including

$$S_{11}^{cal} = -\frac{\Gamma_{33}S_{11}^{meas,L1}S_{11}^{meas,L2} + \Gamma_{11}S_{11}^{meas,L2}S_{11}^{meas,L3} + \Gamma_{22}S_{11}^{meas,L1}S_{11}^{meas,L3}}{\Gamma_{11}S_{11}^{meas,L1} + \Gamma_{22}S_{11}^{meas,L2} + \Gamma_{33}S_{11}^{meas,L3}} \quad (16)$$

$$S_{21}^{cal} = \pm \sqrt{\frac{\Gamma_{L1}S_{11}^{meas,L1}S_{11}^{meas,L2} - \Gamma_{L1}S_{11}^{meas,L1}S_{11}^{meas,L3} - \Gamma_{L2}S_{11}^{meas,L1}S_{11}^{meas,L2} + \Gamma_{L2}S_{11}^{meas,L2}S_{11}^{meas,L3} + \Gamma_{L3}S_{11}^{meas,L1}S_{11}^{meas,L2} - \Gamma_{L3}S_{11}^{meas,L2}S_{11}^{meas,L3}}{\Gamma_{11}S_{11}^{meas,L1} + \Gamma_{22}S_{11}^{meas,L2} + \Gamma_{33}S_{11}^{meas,L3}}} \quad (17)$$

$$S_{22}^{cal} = -\frac{\Gamma_{L1}S_{11}^{meas,L2} - \Gamma_{L1}S_{11}^{meas,L3} - \Gamma_{L2}S_{11}^{meas,L1} + \Gamma_{L2}S_{11}^{meas,L3} + \Gamma_{L3}S_{11}^{meas,L1} - \Gamma_{L3}S_{11}^{meas,L2}}{\Gamma_{11}S_{11}^{meas,L1} + \Gamma_{22}S_{11}^{meas,L2} + \Gamma_{33}S_{11}^{meas,L3}} \quad (18)$$

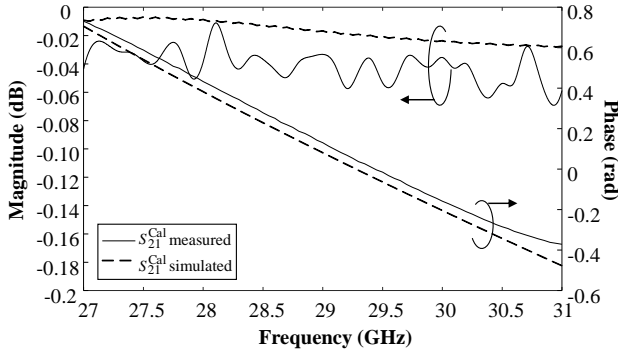


Fig. 8. Magnitude and phase of the transmission coefficient S_{21}^{cal} of the calibration transition. Simulated curves (dashed line) and measured (solid lines) data obtained applying the SCL Method.

surface roughness) of the loads and we calculated these coefficients numerically.

Scattering parameters at the input port 1 of the calibration transition (Fig. 7) are then measured in amplitude and phase connecting at each time the respective shims at port 2 ($S_{11}^{meas,L1}, S_{11}^{meas,L2}, S_{11}^{meas,L3}$). Being the calibration transition a 2-port asymmetrical reciprocal device ($S_{12}^{cal} = S_{21}^{cal}$), the three measurement setups correspond to three equations where the unknowns are the scattering parameters $S_{11}^{adapt}, S_{21}^{adapt}$ and S_{22}^{adapt} of the calibration transition:

$$\begin{aligned} S_{11}^{meas,L1} &= S_{11}^{cal} + \frac{\Gamma_{L1}(S_{21}^{cal})^2}{1 - \Gamma_{L1}S_{22}^{cal}} \\ S_{11}^{meas,L2} &= S_{11}^{cal} + \frac{\Gamma_{L2}(S_{21}^{cal})^2}{1 - \Gamma_{L2}S_{22}^{cal}} \\ (S_{11}^{meas,L3} &= S_{11}^{cal} + \frac{\Gamma_{L3}(S_{21}^{cal})^2}{1 - \Gamma_{L3}S_{22}^{cal}} \end{aligned} \quad (15)$$

By solving this system with respect to $S_{11}^{cal}, S_{21}^{cal}, S_{22}^{cal}$, we obtained the expressions reported in eq. (16)-(18), where we defined:

$$\begin{aligned} \Gamma_{11} &= \Gamma_{L1}(\Gamma_{L3} - \Gamma_{L2}), \\ \Gamma_{22} &= \Gamma_{L2}(\Gamma_{L1} - \Gamma_{L3}), \\ \Gamma_{33} &= \Gamma_{L3}(\Gamma_{L2} - \Gamma_{L1}). \end{aligned} \quad (19)$$

The sign of eq. (17) can be chosen by considering the electrical length of the transition in order to avoid undesired 180° phase delay.

The experimental results of the calibration transition

transmission coefficient are reported in Fig. 8 for both magnitude and phase. The measured data obtained with the described SCL are compared with the full-wave simulation of the calibration transition for validation. The agreement between the curves is quite good with a maximum magnitude and phase error of 0.05 dB and 6.3° , respectively.

The obtained calibration transition scattering parameters are known and the device can be used for the junction J2 characterization in the remaining steps of the calibration procedure (Section III B.2-B.3).

REFERENCES

- [1] Z.-W. Miao, Z.-C. Hao, G. Q. Luo, L. Gao, J. Wang, X. Wang, and W. Hong, "140 GHz high-gain LTCC-integrated transmit-array antenna using a wideband SIW aperture-coupling phase delay structure," *IEEE Trans. Antennas Propag.*, vol. 66, no. 1, pp. 182-190, Jan. 2018.
- [2] H. Yi, S. W. Qu, and C. H. Chan, "Low-cost two-layer terahertz transmit array," *Electronics Letters*, vol. 53, no. 12, pp. 789-791, 2017.
- [3] L. Di Palma, A. Clemente, L. Dussopt, R. Sauleau, P. Potier, and P. Pouliguen, "Circularly-polarized reconfigurable transmitarray in Ka-band with beam scanning and polarization switching capabilities," *IEEE Trans. Antennas Propag.*, vol. 65, no. 2, pp. 529-540, Feb. 2017.
- [4] J. R. Reis, R. F. S. Caldeirinha, A. Hammoudeh, and N. Copner, "Electronically reconfigurable FSS-inspired transmitarray for 2-D beamsteering," *IEEE Trans. Antennas Propag.*, vol. 65, no. 9, pp. 4880-4885, Sep. 2017.
- [5] J. G. Nicholls and S. V. Hum, "Full-space electronic beam-steering transmitarray with integrated leaky-wave feed," *IEEE Trans. Antennas Propag.*, vol. 64, no. 8, pp. 3410-3422, Aug. 2016.
- [6] L. Di Palma, A. Clemente, L. Dussopt, R. Sauleau, P. Potier, and P. Pouliguen, "1-bit reconfigurable unit-cell for Ka-band transmitarrays," *IEEE Antennas Wireless Propag. Lett.*, vol. 15, pp. 560-563, 2016.
- [7] A. Clemente, L. Dussopt, R. Sauleau, P. Potier, and P. Pouliguen, "1-bit reconfigurable unit-cell based on PIN diodes for transmit-array application in X-band," *IEEE Trans. Antennas Propag.*, vol. 60, no. 5, pp. 2260-2269, May 2012.
- [8] C. Huang, W. Pan, X. Ma, and X. Luo, "1-bit reconfigurable circularly polarized transmitarray in X-band," *IEEE Antennas Wireless Propag. Lett.*, vol. 15, pp. 448-451, 2016.
- [9] L. Di Palma, A. Clemente, L. Dussopt, R. Sauleau, P. Potier, and P. Pouliguen, "Circularly-polarized reconfigurable unit-cell for transmitarray applications in Ka-band," in *Proc. IEEE Int. Symp. Antennas Propag. (APSURSI)*, Fajardo, Puerto Rico, Jul. 2016, pp. 1411-1412.
- [10] MM-Microwave. Available online: www.sylatech.com.
- [11] Baker-Jarvis J, Janezic MD, Grosvenor JH Jr., Geyer RG, NIST Tech. Note 1355-R, 1993
- [12] Baker-Jarvis J, NIST Tech. Note 1341, 1990
- [13] V. B. Bregar, D. Lisjak, A. Nidarsic and M. Drogenik, "Experimental analysis of short-circuit line technique for measuring permeability of ferromagnetic materials," *Proc. 64th ARFTG Microwave Meas. Conf.*, 2004, pp. 117-123.